Initial tests and runs with the ES-III RF-funnel prototype

Dan Fudenberg[*], Thomas Brunner[†]

May 28, 2014

Contents

1 Introduction

This document describes the most recent tests we performed with the RF funnel setup at Stanford. The purpose of this document is to create a reference for internal use, share our current experimental

[*]dfudenb@stanford.edu
[†]tbrunner@stanford.edu

status and trigger discussions. A schematic of the setup is shown in Fig. 2 of arXiv:1302.6940v1. All error bars shown in this document are one standard deviation of the data aggregated in one second intervals over the integration time. The integration time varied in various measurements.

The central device of our setup is the RF funnel that is installed in a large vacuum chamber, so-called chamber B. Upstream of the funnel in chamber A, a Gd-driven Ba-ion source produces ions in a gaseous environment at pressures of up to 12 bar. These ions are flushed through a nozzle and enter the funnel in a gas jet. While the neutral gas is pumped out through the spacing between the funnel electrodes, the applied RF confines the ions to the inner conical region of the funnel. Residual gas flow flushes the ions through an aperture of 1 mm diameter (at ground potential) into the downstream chamber, so-called chamber C. There, the ions are captured by a sextupole ion guide (SPIG) and guided through another differential pumping barrier before they are detected in the final chamber of the setup (so-called chamber D). The ions are detected by a channeltron (CEM). All measurements so far were performed using either Xe or Ar gas.

The properties of the setup during gas-jet operation have been studied. The ion-count rate at the detector has been measured as a function of gas pressure in chamber A and various RF amplitudes applied to the RF-funnel. This is described in Section 3. In further studies the properties of ion transmission at an increased stagnation pressure in chamber B was investigated. These results are presented in Section 4.

The described setup is designed as a UHV vacuum system. The used materials are all UHV-compatible. Four viton O-rings are installed in the system (one at the source holder, one at the aperture between chambers B and C, and two at the biased aperture between chambers C and D). In addition to these, the cryo pump cold head is sealed with O-rings as well. All chambers can be pumped through turbo-molecular pumps. The base pressures of chambers B, C, and D typically reach $9{\cdot}10^{-9}$ Torr, $2{\cdot}10^{-9}$ Torr, and $4{\cdot}10^{-9}$ Torr, respectively, after two weeks of pumping. Pressures in the high 10^{-10} Torr range were achieved in chamber C after several weeks of continuous pumping.

2 Setup

To recover xenon, the setup was designed around a large-diameter vacuum chamber (20 inch diameter) mounted on top of a cryopump (Sumitomo Marathon CP-20 Cryopump). For maximum pumping speed in the volume surrounding the RF-funnel, the funnel is centered in the vacuum chamber above the cryopump, and aligned along the diameter of the chamber between two CF8" access ports at 0° and 180°. The turbo pump to evacuate the chamber prior to cooling the cryopump is installed at CF8" port at 270°. This turbo pump is valved off by a gate valve during gas operation.The placement of the funnel in the center of chamber B required an ion guide in chamber C that bridges a distance of almost half a meter. Chamber C is differentially pumped by the mag lev turbo pump. A SPIG was chosen to guide the ions through this differential pumping stage. A picture of the SPIG prior to its installation is shown in Fig. C.4.

2.1 Gas operation modes

Although the goal is to understand the performance of the system at extracting ions from Xe gas, the setup has been operated with both Xe and Ar gas. The operation with an Ar gas jet is more convenient since the gas is not recovered. This allows for faster turn around time. Furthermore, the supply of Xe gas is limited to 1.5 kg while the Ar bottle contains larger amounts of gas, hence,

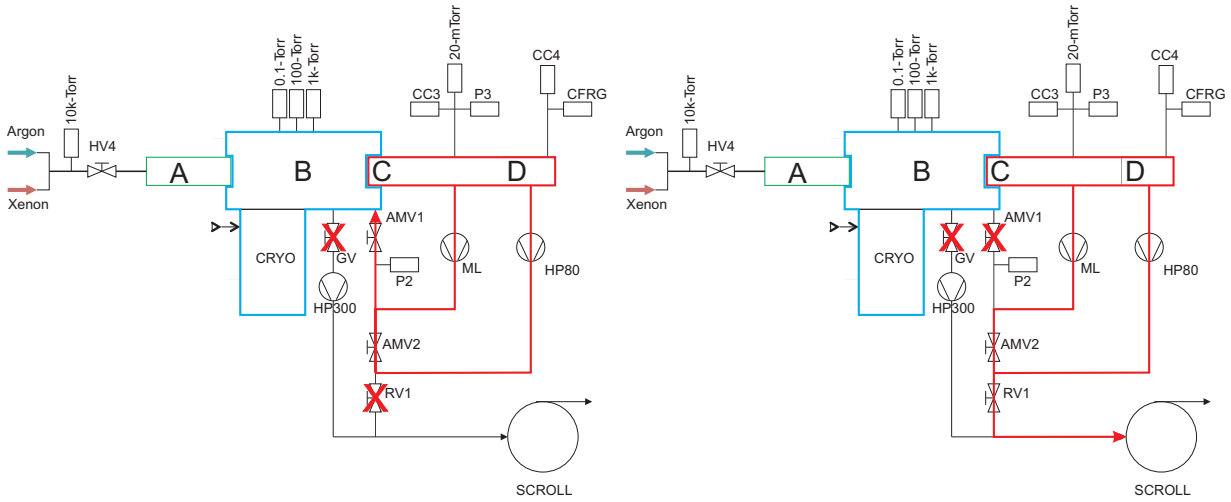

(a) Recovery pumping scheme.

(b) Non-recovery pumping scheme.

Figure 2.1: Pumping setup and schemes that we used for the presented tests. Argon or Xenon gas can be supplied to the setup as indicated on the left by the green and red arrows, respectively. The vacuum system is separated into three main sections, the high-pressure section (in green, consisting of chamber A), the funnel section, and main chamber, pumped by the cryo pump (in blue, consisting of chamber B), and the downstream vacuum section (pumped by turbo pumps ML (mag lev) and HP80 (HiPace80) in red, consisting of chambers C and D). The red crosses indicate closed valves during a certain mode of operation. In recovery mode, the gas from chambers C and D is compressed into chamber B where it freezes to the cryo pump. In non-recovery mode, the gas from chambers C and D is pumped to atmosphere through the scroll pump.

one can operate the gas jet for an extended period of time with Ar.

There are two main modes of operation for the setup: recovery and non-recovery mode. In recovery operation mode all gas is frozen to the cryo pump and can be recovered: the exhausts of turbo pumps ML and HP80 (see Fig. 2.1a) are fed back into chamber B through all-metal-valve 1 (AMV1). The pressure in chamber B acts as fore-vacuum for the turbo pumps. All Xe measurements and some Ar measurements were performed in this mode. However, only Xe gas was recovered after a run; Ar was pumped to atmosphere.

During non-recovery operation mode, AMV1 is closed and the fore-line of turbo pumps ML and HP80 is evacuated by the scroll pump. In this mode of operation only the gas leaving through the funnel-electrode spacing freezes to the cryo pump. Gas that flows into the downstream chambers is pumped to atmosphere. This mode of operation has only been used when measuring with Ar gas, or pumping down to vacuum prior to any gas operation. The advantage running in this mode is that the scroll pump provides the fore-line pressure for the turbo pumps on chambers C and D and is thus independent of the pressure in chamber B. A simplified schematic of this pumping mode is shown in Fig. 2.1b.

It was discovered that the cold cathode gauges in chambers C and D create ions that could be detected by the CEM when running with Argon or Xenon gas. These ions could be detected by the CEM when running with Argon and Xenon gas. In all runs prior to February 2014, all cold cathode gauges were turned off during gas operation. At the beginning of April 2014, chicanes,

consisting of two or three 90° turns, were installed between the cold cathode gauges and the flight path of the ions in vacuum chambers C and D. These chicanes make the count rate at the CEM independent of the operation of the cold cathode gauges (see Fig. C.8). The cold cathode gauge in chamber B is turned off during all gas operation because the pressure is too high.

2.2 High pressure chamber A and ion source

The pressure in the high pressure chamber A upstream of the nozzle is set by a pressure regulator. The Xe system has a regulator installed in the supply line while the pressure regulator at the Ar bottle is used to set the pressure. Both, Ar and Xe gas have their own purifier[1]. The Xe lines are evacuated prior to a measurement, whereas the Ar lines are pumped and purged by a separate scroll pump bypassing the purifier. Once the lines have been pumped and purged at least three times, the gas is redirected through the purifier and the lines pumped and purged an additional two times with purified gas.

All measurements described in this document were performed using a non-symmetric ion source assembly. The source is installed in this assembly perpendicular to the gas flow in chamber A right at the entrance of the converging-diverging nozzle. Tests with a dummy source plate (no radioactive source deposited) and a ^{148}Gd-driven Ba ion source were performed. A picture of the source holder – that was installed in all measurements – with source plate installed is shown in Fig. C.1. The black (baked) viton O-ring ensures that gas has to flow across the source plate surface. It prevents gas from bypassing the source assembly. A sectioned view of the source installed at the nozzle is shown in Fig. C.2. The current source holder design is not ideal due to the lack of rotational symmetry. A new source design concept is being developed. However, as long as m/q of the ions produced by the current source is unknown, the source holder will not be replaced.

In the ^{148}Gd ($Q = 3183\,\mathrm{keV}$) driven Ba-ion source, Ba-ions are knocked out of a BaF coating by the recoil of the daughter nucleus[2]. The α-source activity is $\sim$244 Bq. Considering an acceptance of 50% and assuming a Ba(F)-ion production rate of (5-10)% one expects to generate $\sim$6-12 Ba(F)-ions per second. However, count rates as high as several thousand ions per second were detected when operating the RF funnel with Ar and Xe gas. To investigate the origin of this high count rate, SRIM2013 simulations were performed focusing on the energy loss of α particles through ionization in the Xe gas. These simulations were performed for Xe pressures from 1 bar to 10 bar in 1 bar increments. This α-energy loss is shown in Fig. 2.2a for a gap of 0.76 mm between source surface and source holder wall as is present in the setup. The number of Xe ions produced by an α particle in this 0.76 mm range is shown in Fig. 2.2b assuming a Xe-ionization energy of 21 eV and completely neglecting electron-ion recombination. The intention of this plot is to illustrate that one α particle will produce a large amount of secondary ions. The composition of these ions then also depends on impurities in the applied gas.

2.3 Funnel RF generation

The RF funnel is driven by an Agilent 33120A frequency generator that is connected to an ENI A150 amplifier through an attenuator, typically 20dB, (as the smallest amplitude the function

[1] Xe purifier: SAES MC400-903
O_2, H_2O, CO, CO_2, H2 < 10 pptV
Acids, Bases, Organics, Refractory Compounds < 1 ppbV

[2] Review of Scientific Instruments 81(2010)113301

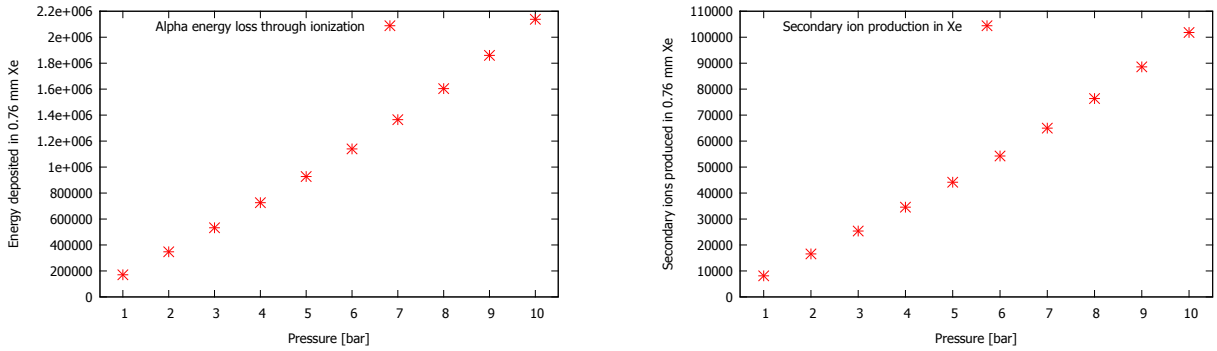

(a) Energy loss through ionization.

(b) Expected number of produced Xe ions.

Figure 2.2: SRIM2013 simulation of $Q = 3183\,\text{keV}$ α particles in 0.76 mm Xe.

generator outputs is $50\,\text{mV}_{\text{PP}}$). This amplifier is then connected to a balun (Balun Design Model 1413t 1:4/3 kW) which is connected to the funnel. During initial tests, it was determined that longer cable length between the amplifier and balun increased power lost and hence reduced the maximum V_{PP} attainable on the funnel. To reduce losses the balun is directly connected to the amplifier through a barrel connector (see Fig. C.3). The output at the balun is not symmetrical. During operation the voltage is measured by a scope with a 1:100 probe with $1\,\text{M}\Omega$ input termination. The voltage amplitude of the funnel is calculated as the voltage difference between the phases at the balun scaled to the voltage that reaches the funnel. This behavior is shown in Fig. 2.3a. The measurement of this ratio is described below. Typically, the RF funnel is supplied with a sinusoidal wave at a frequency of 2.6 MHz at various amplitudes of up to $97.5\,\text{V}_{\text{PP}}$, where the amplifier outputs 120 W. All voltages stayed well below the break-down voltage (see Paschen curves in Figs. B.1 and B.2).

The funnel itself has a capacitance of about 6.041 nF at 1 kHz and 6.051 nF at 10 kHz (March 4, 2013, measured in vacuum through SHV feed throughs - the capacitance changes only marginally with gas flow). Its resonance frequency is close to 2.6 MHz. The voltage on each of the funnel-electrode stacks versus that applied at the output of the balun was measured (on June 14, 2013) with the funnel installed in the center of chamber B and the system open in atmosphere. As shown in Fig. 2.3a, the voltage on each phase was measured for several driving voltages supplied by the function generator. The V_{PP} across the funnel stacks (2-1) was compared to that across the balun phases (4-3), and a constant ratio observed at each frequency. These measurements were repeated and a ratio determined for several frequencies, as shown in Fig. 2.3b.

2.4 SPIG

The SextuPole Ion Guide (SPIG, see Fig. C.4) has a capacitance of 88.9 pF and 89.64 pF at 1 kHz and 10 kHz, respectively. The frequency is generated by a Hewlett Packard 3325B function generator and then amplified by an ENI 240L amplifier. This signal is then connected to the primary side of a toroid. The SPIG is connected to the secondary side of the toroid. The secondary side of the transformer toroid can be biased and thus the SPIG can be floated to various voltages. The SPIG is typically operated at 2 MHz and $200\,\text{V}_{\text{PP}}$. A scan of the SPIG RF amplitude is shown in Fig. 2.4. A scan of SPIG DC floating voltages is shown in Fig. 2.5a and Fig. 2.5b for Xenon and Argon,

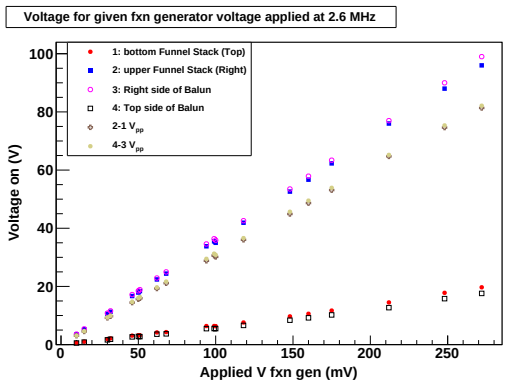

(a) Voltage measured on funnel segments (labeled 1 and 2) and at the output of the balun (3 and 4). Also shown is the effective amplitude V_{PP} at the funnel, labeled 2-1, and at the balun, labeled 4-3.

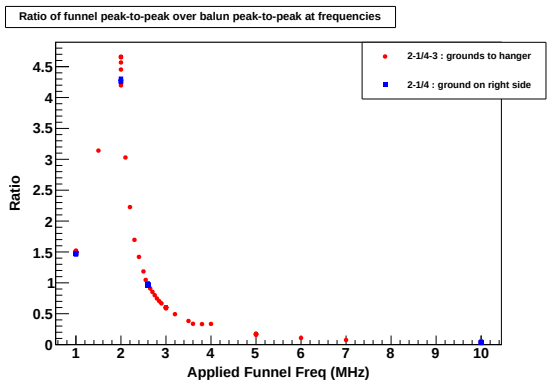

(b) Ratio of funnel peak-to-peak amplitude versus balun peak-to-peak amplitude as a function of the radio frequency. Typical operation with the funnel is at 2.6 MHz.

Figure 2.3: Properties of the RF-funnel. Shown are the voltage at the funnel (a) as a function of function generator amplitude and (b) the ratio of voltages at funnel and balun as function of the applied frequency.

respectively. In Xenon gas at positive voltages, the SPIG repels the ions and no ion signal at the downstream CEM can be detected; in Argon, scans show very few counts but still nonzero. For slightly negative DC bias on the SPIG ions are sucked into the SPIG and guided through chamber C. Typically, the SPIG is biased to -5.7 V. Ions undergo collisions with residual gas in chamber C losing most of their kinetic energy (see Fig. B.3 for mean-free-path in Xe and Ar gas). As a result, the ions inside the SPIG are thermalized at a potential of -5.7 V. Hence, a ground potential is repulsive for ions leaving the SPIG. This has been verified by scanning the downstream aperture. A voltage negative enough to bridge the distance between SPIG and downstream aperture has to be applied in order to extract ions from the SPIG. Typically, the downstream aperture is biased at -220 V.

During measurements, the null-hypothesis, i.e., that all observed ions originate from the funnel, is tested by reducing the RF amplitude on the SPIG to a few mV. If all detected ions originate from the high-pressure chamber A and the funnel, the count rate drops to zero.

2.5 CEM and trigger setup

The ions in all tests were detected using either a DeTech 2403 or a DeTech 402AH3 channeltron. The channeltron was either read out through an ORTEC VT120A fast preamp before April 04, 2014, or an ORTEC fast timing amplifier model 474 afterward, before the counts were counted with a Stanford Research time interval/frequency counter (SR620). The channeltron was operated in two modes, either in normal mode where the current at the anode was directly fed to the amplifier, or in capacitively decoupled mode, where the signal was first decoupled from the applied positive high voltage through a RC circuit. Both methods are illustrated in Fig. 2.6's schematics. In all the scans until April 2014 the SR620's trigger threshold was set to -0.020 V.

The channeltron was biased with a potential difference of 1.8 kV to 2.1 kV across it. In initial tests the normal operation mode of the channeltron was used with the front part of the CEM

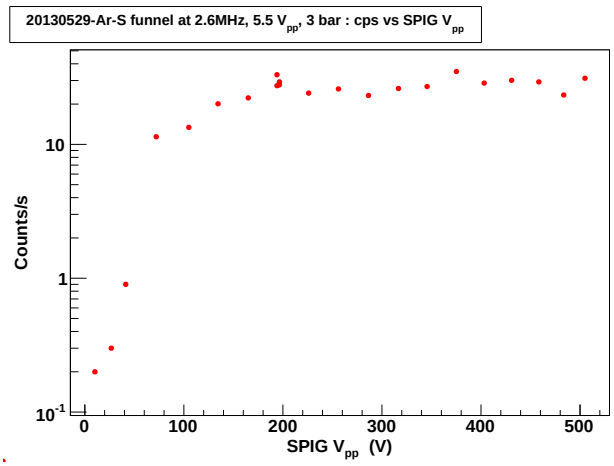

Figure 2.4: SPIG-RF amplitude scan. Displayed is the count rate on the CEM as a function of SPIG RF amplitude (V_{PP}). In all the following experiments the SPIG is operated at 2 MHz and 200 V_{PP}. The scan was recorded with 3 bar (∼2300 Torr) Ar gas, Ba-ion source and the RF funnel at 2.6 MHz and 5.5 V_{PP}.

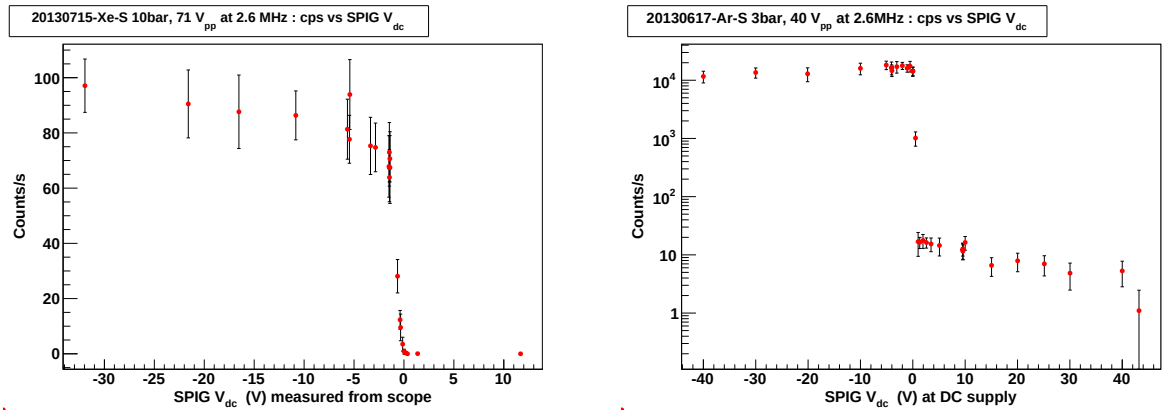

(a) Xenon at 10 bar, RF funnel at 2.6 MHz/71 V_{PP}. (b) Argon at 3 bar, RF funnel at 2.6 MHz/40 V_{PP}.

Figure 2.5: Scan of the DC voltage applied to the SPIG (floating voltage). For positive potentials, almost no ions pass through the SPIG (2 MHz, 200 V_{PP}).

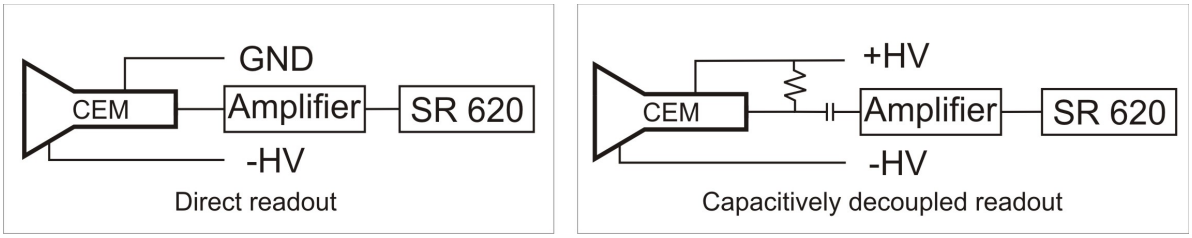

Figure 2.6: Schematic of the channeltron (CEM) readout in normal (left) and capacitively decoupled (right) mode. Typically, a potential difference of 1.8 kV to 2.1 kV was applied to the channeltron. The amplifier was an ORTEC VT120A or an ORTEC fast timing amplifier model 474.

biased negative to attract and focus ions. In later tests the front of the CEM was biased with a low negative voltage on the front section (typically -10 V) and +2 kV bias on the center and rear segments. The CEM's signal was then capacitively decoupled from the high voltage before it was amplified. The capacitively decoupled method was mainly used to tune and optimize the ion optics in order to potentially inject into a RGA quadrupole. It is noted here that it was possible to optimize the ion count rate at the CEM in capacitively decoupled mode to the same order of transmission as in the normal mode. However, ions could never be injected into a RGA, positioned at the same spot, and successfully detected.

3 RF-amplitude scans

In initial measurements various parameters were scanned while recording the count rate at the CEM. Both, Xenon gas and Argon gas were used. All measurements presented in this section were performed in recovery pumping mode (see Fig. 2.1a); where the gas reaching chambers C and D was compressed back into chamber B where it froze onto the cryo pump. These measurements were taken over short time periods, typically less than 20 minutes. A measurement period consisted of: first, the gas valve was opened (HV4 in Fig. 2.1a). Then the gas jet was given a short period of time to stabilize before count data was collected. Finally, after finishing count collection, the gas was closed off again, typically at HV4, and the next run was not started until the temperature of the cryo pump had settled.

The goals of these measurements were (i) to confirm ion production by the ion source and the ability to extract these into vacuum, and (ii) to understand and optimize the operation of the funnel. The measurements are intended to be compared to Victor Varentsov's simulations. The main levers used to investigate the operation of the funnel are the pressure in the chamber A, and the applied RF-voltage. The RF-voltage is usually applied at 2.6 MHz; higher frequencies are simulated to have higher efficiencies, however the voltage that can be applied to the funnel is restricted at higher frequencies, hence measurements at higher funnel frequencies were not possible. A selection of results from these scans is presented in the following subsections.

3.1 Xenon

The count rate was recorded as function of applied funnel RF-amplitudes while applying gas to chamber A. After initial confirmation of ions coming through the funnel with the ^{148}Gd-driven ion source, a series of runs was performed with the Ba-ion source holder installed but with neither

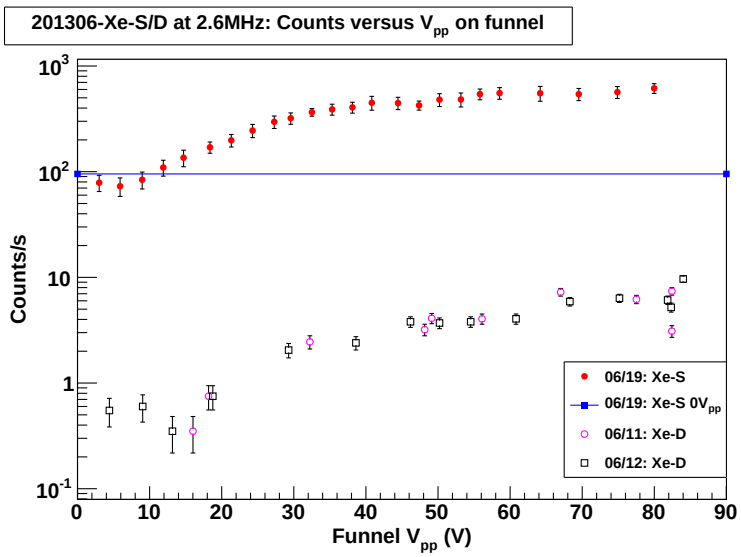

Figure 3.1: Count rate on the channeltron as a function of applied RF-funnel voltage at 2.6 MHz. Data was recorded with either the ^{148}Gd-driven Ba-ion source (Xe-S) or the dummy source (Xe-D). The horizontal line indicates the count rate with no RF applied (Xe-S). These measurements were recorded at 10 bar (∼7600 Torr) in chamber A.

^{148}Gd nor BaF plated onto the source plate (see Fig. C.1). In this setup, 10 bar of Xe was applied to chamber A and the funnel's RF amplitude was scanned. The resulting count rate is shown in Fig. 3.1 (crosses and empty squares). It was noted that ions are created somewhere in the region of nozzle and funnel. When the SPIG was turned off, the count rate dropped to zero, ruling out ion creation downstream of the SPIG. If the ions were originating from the SPIG, they should not show any dependence on the applied RF-funnel amplitude. Together, this is a strong argument that the ions seen with the dummy source actually pass through the RF-funnel, suggesting they are generated before or in the converging-diverging nozzle.

With the ^{148}Gd-driven Ba-ion source installed, the count rate is significantly increased (see red dots in Fig. 3.1). It is noted that ions from the source are detected at the channeltron even when no RF is applied to the funnel. Without confining RF applied to the funnel, the ions are expected to follow the flow of the gas. Thus, only ions that were flushed through the funnel with the neutral gas atoms will be captured and guided by the SPIG to the CEM. If no RF is applied, ions just flow with the gas. With RF voltage applied to the funnel, the count rate increased by about an order of magnitude.

In consecutive studies, the RF amplitude applied to the funnel was varied at various Xenon-gas pressures in chamber A. During these tests the pressures in the downstream chambers were not monitored, as the pressure was out of range on the sensors that were then installed, however, each measurement was started only after the cryo pump cooled down again. Each measurement series at one specific pressure only took several minutes. The resulting curves are shown in Fig. 3.2. The applied Xe pressures in chamber A are listed in the legend in decreasing order.

A scans performed over a larger set of pressures and applied voltages are shown Figures 3.3, and 3.4. Here, the pressure was adjusted and HV4 opened, then after a short waiting period the amplitude scan was started. Before a new scan was started the second stage of the cryopump was

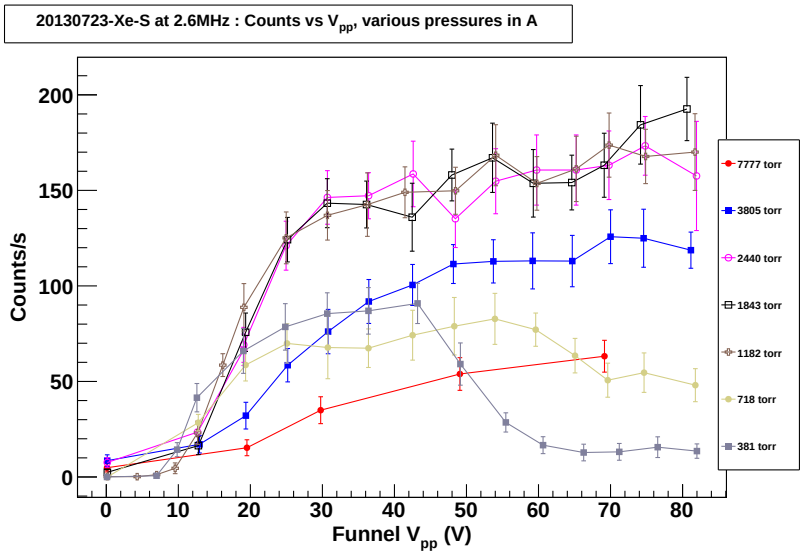

Figure 3.2: Count rate as function of applied RF-amplitude at 2.6 MHz. These scans were recorded for different pressures, listed in the legend, in chamber A.

allowed to cool down again. All measurements were performed running with Xenon gas. Figure 3.3 was recorded at a funnel frequency of 2.6 MHz. A set of measurements performed at a lower frequency, 1 MHz, to achieve higher voltage on the funnel (207 V_{PP}), is presented in Fig. 3.4.

3.2 Argon

These Argon scans were performed similar to the Xenon scans. All measurements presented in this section were performed applying the recovery pumping scheme (see Fig. 2.1a). The gas in chambers C and D was compressed back into chamber B by the turbo pumps. However, the Argon gas used in these runs was not recovered. Typically at the end of the day, the cryo pump was warmed up. Once the pressure in chamber B rose above the base pressure of the scroll pump, the gate valve was opened and the vaporized Ar gas pumped out through the scroll pump. The turbo pumps were all turned off at this time. The turbo pumps on the system were turned back on once all the Ar gas boiled off the cryo pump (after both stages were above ∼90 K). At this point, the cryo pump was turned back on again to cool down for the next set of measurement.

Similar to the runs with Xe, Ar gas was injected into the system and the count rate was measured as a function of RF-amplitude applied the the funnel. This measurement was performed with and without a ^{148}Gd-driven Ba-ion source. Similar to the case in Xe, ions were detected at the CEM even with no ion source installed. Once the ion source was installed, the ion count rate increased by four orders of magnitude. There was a three order of magnitude increase in counts achieved with RF-voltages over without. This is shown in Fig. 3.5. It was again verified in both cases that ions were not produced downstream of the SPIG by turning it off and observing the count rate: with it off the ion count rate dropped to zero.

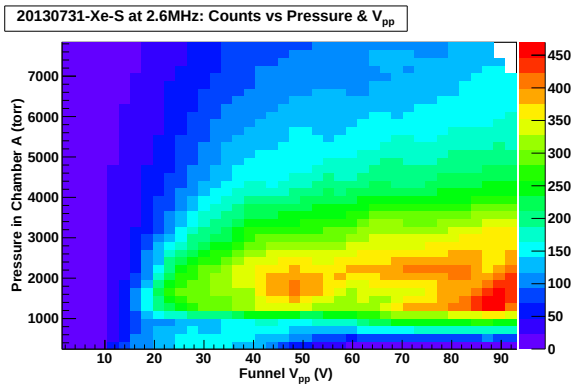

Figure 3.3: Count rate as function of RF amplitude and input pressure in chamber A at 2.6 MHz.

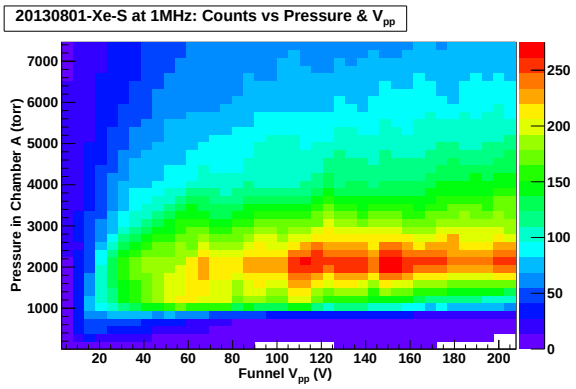

Figure 3.4: Count rate as function of RF amplitude and input pressure in chamber A at 1.0 MHz.

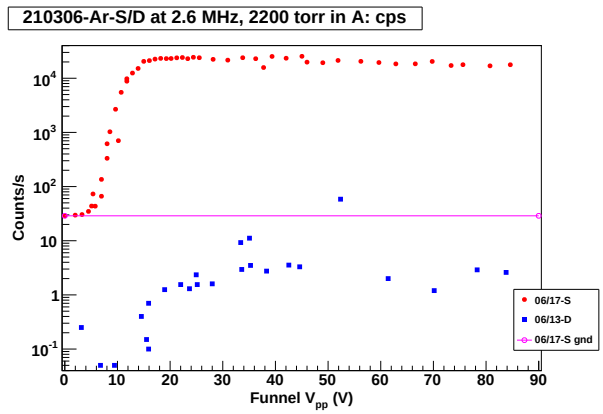

Figure 3.5: Amplitude scan of the RF-funnel voltage. Shown is the count rate as a function of applied voltage with and without a ^{148}Gd-drive Ba-ion source.

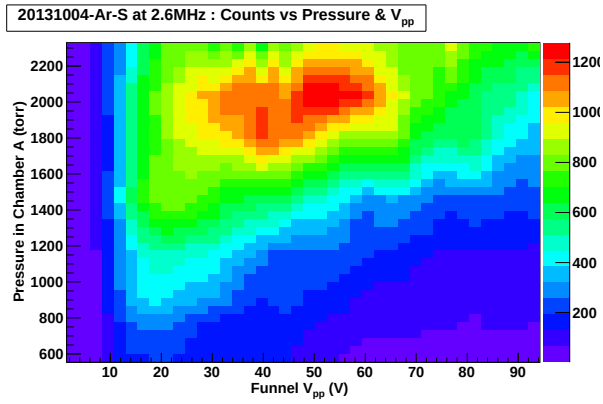

Figure 3.6: Intensity map of the CPS measured in Argon with Ba-ion source and funnel RF at 2.6 MHz. The plot shows a scan of funnel RF amplitude at various pressures.

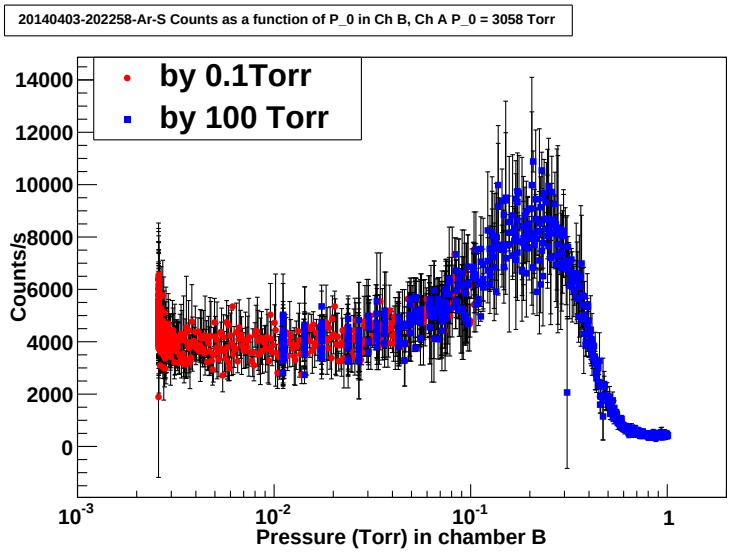

Figure 4.1: Counts per second on the CEM as a function of pressure in chamber B for a constant input pressure of 3058 Torr in chamber A. The red circles are data points recorded by the 100 mTorr Baratron while the blue squares were recorded with the 100 Torr Baratron. Both gauges overlap between 10 mTorr and 100 mTorr. Later plots use an interpolated pressure where the 100 mTorr Baratron values are used while the pressure is below 100 mTorr and the 100 Torr Baratron is used above.

4 Stagnation-pressure measurements with Argon

Victor suggested measuring the dependence of the pressure in chambers C and D and the count rate depending on the pressure in chamber B. The pressure measurement setup was modified in order to enable these measurements. One major improvement was the installation of at least two 90° bends between the cold cathode gauges and the ion flight path. Prior to this upgrade, the cold cathode gauges would produce ions that were then detected by the CEM, especially during gas operation. Hence, in prior measurements the cold cathode gauges were turned off. With the bends installed the cold cathode gauges can now be operated during gas jet operation without having any effect on the count rate.

In the initial tests a 100 Torr and a 20 mTorr Baratron gauge were installed on chamber B. On April 2nd, 2014, the 20 mTorr Baratron previously mounted on chamber B was moved to chamber C and a 100 mTorr Baratron was installed at its place on chamber B. The location of the 100 Torr Baratron is indicated in Fig. C.6 and the locations of the 100 mTorr and the 1 kTorr Baratron are shown in Fig. C.7. This configuration provides a more detailed measurement of the pressures in chambers B and C. The pressure range covered by each Baratron in chamber B is illustrated in Fig. 4.1 (the 100 mTorr Baratron reads up to 104 mTorr). The horizontal accumulation of blue points in the 10s of mTorr regime of the 100 Torr Baratron is due to the digitizer that converts the voltage output of the Baratron to a digital value.

The stagnation pressure surrounding the funnel directly influences the shape of the gas jet and hence the ion transmission through the funnel. In the current setup the pressure in chamber B cannot be controlled directly. The cryo pump is constantly operating at full cooling power.

However, by constantly loading the cryo pump with gas, the temperature of the cryo pump and hence the pressure in chamber B increases. In order to test the influence of the stagnation pressure on the ion transmission and gas flow through the system, the ion count rate was measured as a function of pressure in chamber B. All of these tests were performed with Ar gas in non-recovery mode (see Fig. 2.1b) in order to reach higher pressures in chamber B without unduly taxing the turbo pumps of chambers C and D. During these measurements the pressures in all chambers have been recorded as well as temperatures on the cryo pump and ion count rate. The lowest input pressure in chamber A was 2458 Torr. An input pressure of 1555 Torr was also tested, however, the gas flow was too little to increase the pressure in chamber B within a reasonable amount of time.

It shall be noted here that the cryo pump went through a cooling cycle in the night of April 9 to 10, 2014. All (the majority of) Ar gas that had been frozen to the pump on April 9^{th} was pumped out of the system. On April 10^{th} the chamber was first evacuated with turbo pumps before the cryo pump was turned on. The measurements were started after lunch once the cryo pump had cooled down completely (45 K and 10 K on first and second stage, respectively).

4.1 Temperature behavior

The temperature behavior of the cryo pump as a function of pressure in chamber B is shown in Figures 4.2a and 4.2b for first and second stage of the cryo pump, respectively. As long as the pressure in chamber B is below the sublimation curve, the temperature of the second stage increases while the pressure stays constant. This constant pressure only depends on the input pressure in chamber A, i.e., the higher the pressure in chamber A the higher the lowest stagnation pressure in chamber B. Once the temperature of the cryo pump is higher than the sublimation temperature, the temperature increases following the sublimation curve[3] (see Fig. 4.2b). The behavior of the cryo pump stages is more consistent for the second stage than it is for the first stage. This might be due to two facts: (i) the first stage is closer the funnel and so is loaded heavier with Ar gas, and thus the time the measurement is performed, i.e., the amount of Ar gas frozen to the pump, has a direct impact on the slope and (ii) the initial temperature of the stage has a direct influence on the measurement as well. In several studies a new gas run was started as soon as the first stage reached a temperature of ∼55 K. These runs start with the 1^{st} stage temperature still falling, see Fig. 4.2a.

The cryo pump temperature of first versus second stage is presented in Fig. 4.3. The initial shape of the curve at low temperatures on the second stage mainly depends on the initial temperature on the first stage (typically ∼11 K) when a gas run was started. Once the temperature on the second stage passes 45 K to 50 K, the temperatures rise at the same rate. The rate of rise of the graph depends on the applied pressure in chamber A. The graph rises steeper for low input pressures and becomes shallower for higher input pressures.

4.2 Pressure behavior

The pressure of chamber C as a function of pressure in chamber B is shown in Fig. 4.4. In the first measurements, only pressures of up to 1 Torr were tolerated in chamber B. In later runs a pressure of up to 10 Torr was accepted in chamber B. It is interesting to observe that the pressure in the downstream chamber is not monotonic with pressure in B. First there is a slow change with pressure, for low pressure in A initially decreasing, while for high pressure in chamber A

[3] The Journal of Chemical Thermodynamics 40(2008)1621

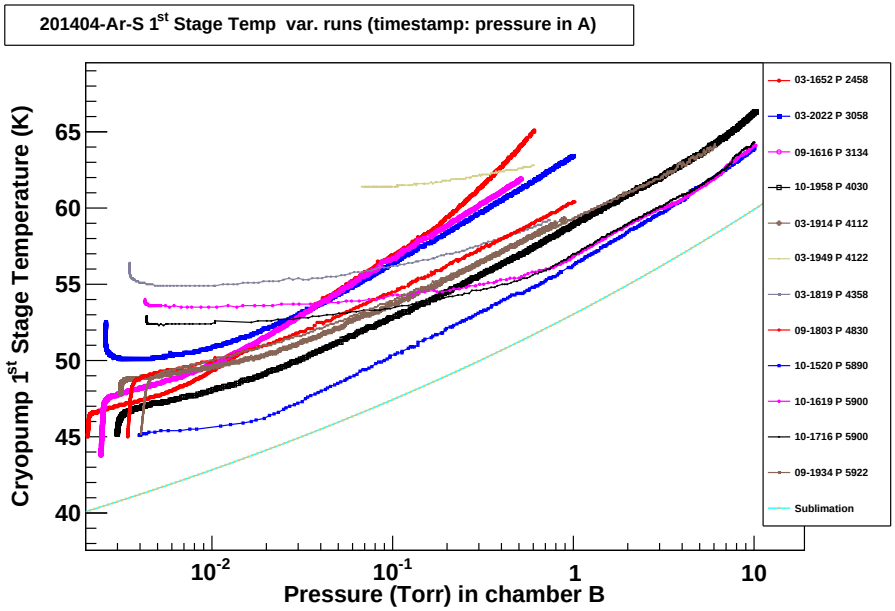

(a) 1st stage temperature.

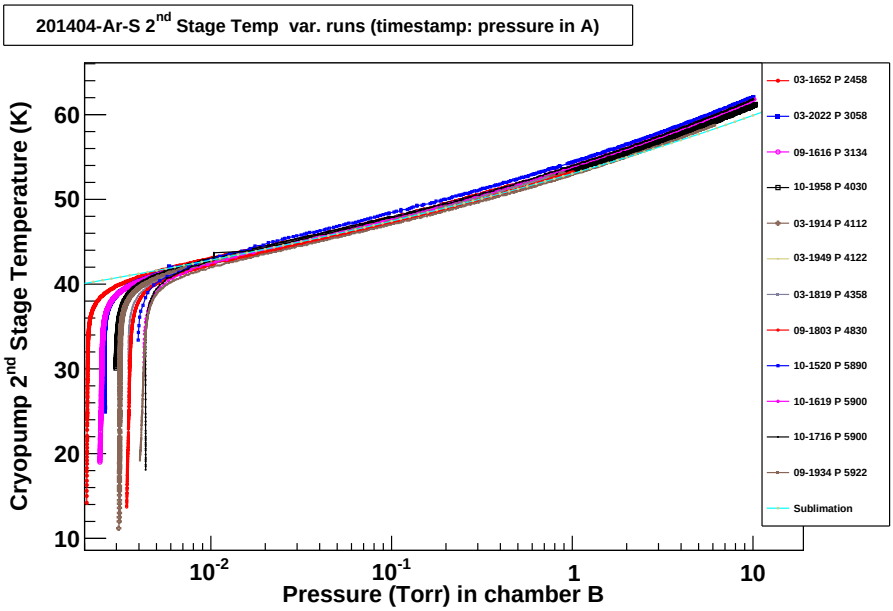

(b) 2nd stage temperature.

Figure 4.2: Temperatures of cryo pump stages versus pressure in chamber B. The legend name is dd-hhmm P *pressure in Torr* of chamber A with dd being the day in April, 2014, and hh and mm being hour and minute when the scan was started, respectively. The scans are arranged in increasing order of input pressure. The dotted cyan line shows the sublimation curve of Ar (from The Journal of Chemical Thermodynamics 40(2008)1621).

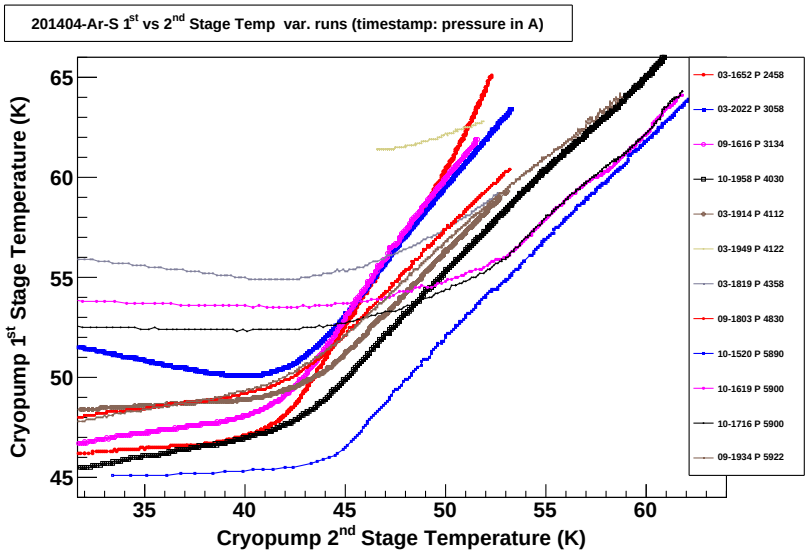

Figure 4.3: Temperatures of 1st stage versus 2nd stage. Runs labeled as in Fig. 4.2.

initially increasing then suddenly decreasing. After reaching a minimum pressure, the pressure increases quickly to a maximum pressure which is typically reached at around 1.5 Torr stagnation pressure in B. Afterwards, the pressure starts decreasing again until it reaches a second minimum at around 4 Torr after which the pressure starts increasing again. On the first pressure decrease, a sub-structure is present. The dominance and location of this substructure depends on the inlet pressure in chamber A. The higher this inlet pressure, the more dominant the sub-structure is present. Furthermore, the location of the structure is pushed to higher stagnation pressures for increased inlet pressures. The sub-structure appears in the range between 12 mTorr and 35 mTorr and it starts with a sudden drop in downstream pressure. For input pressures below ∼4830 Torr a steep upward step follows the downward step after an increase of ∼5-10 mTorr in stagnation pressure.

4.3 Count-rate behavior

The CEM setup is described in Section 2.5. The measurements recorded on April 3rd were recorded with the Ortec VT120A in normal operation with -2000 V/GND/GND applied to the channeltron. The scans from April 3rd are shown in Fig. 4.6a. Due to a hardware failure the system was changed after these measurements and the CEM signal was fed to an ORTEC fast timing amplifier model 474. The CEM was operated in capacitively decoupled mode with a bias of -10/+2032/+2032 V. The effect of the trigger threshold was investigated systematically with a LabView program with this new amplification. The trigger threshold was scanned while running gas through the funnel with the SPIG RF turned on or off. Argon gas was applied to chamber A during these measurements. The results of the scan are shown in Fig. 4.5 with the chosen trigger threshold of -0.030 V indicated by a vertical blue line. All measurements that were recorded on April 9th and 10th used the same setting and similar voltages on the CEM and can be compared directly. The pressure scans from April 9th and 10th are shown in Fig. 4.6b.

When looking at Fig. 4.6a one can conclude that lower pressures in chamber A (in the current

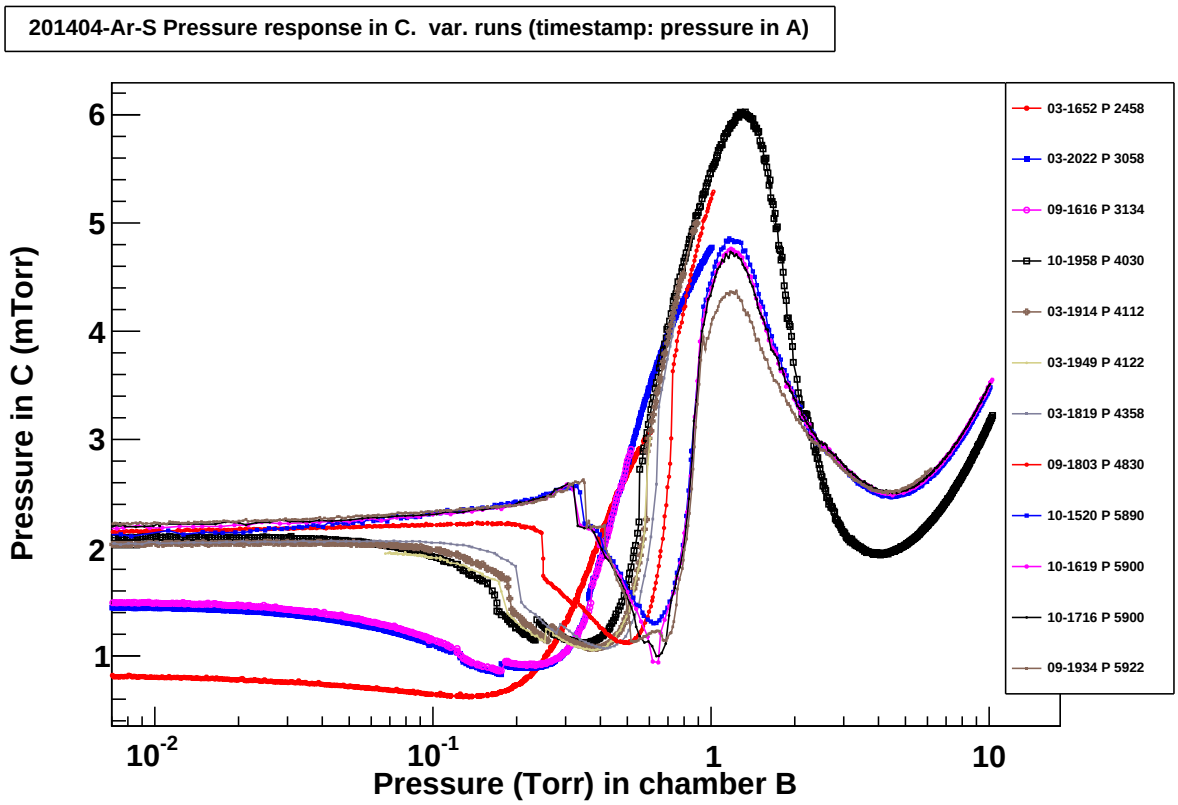

Figure 4.4: Pressure in chamber C read by the 20 mTorr Baratron as a function of pressure in chamber B. Runs labeled as in Fig. 4.2.

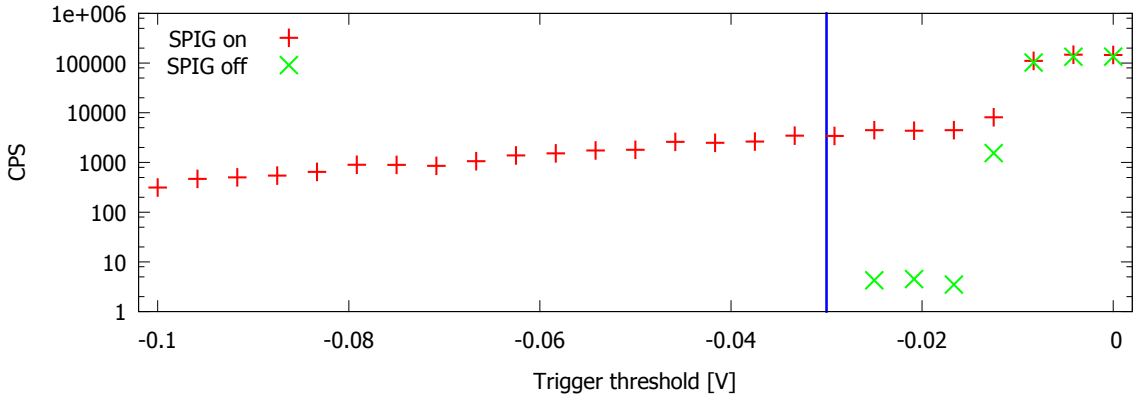

Figure 4.5: Counts per second (CPS) as a function of trigger threshold for both SPIG RF on and off. Both scans were performed with Ar gas flow. The chosen trigger threshold of -0.030 V is indicated by the blue vertical line. Zero CPS are omitted.

case 2458 Torr and 3058 Torr) are favorable compared to input pressures of more than 4000 Torr for a RF confinement of 20 V_{PP} at 2.6 MHz. A similar behavior was also found on April 9/10 as shown in Fig. 4.6b. There, the highest ion count rate was also obtained for lower pressures, but the effect of changing pressure was reduced with greater RF-voltage applied. Fig. 4.6b also shows scans with RF funnel amplitudes of 0 V, and 77 V. Even with zero Volt applied to the funnel ions are pushed through it. However, applying a RF frequency to the funnel creates a confining potential and increases the transmission through the funnel.

Scans were performed with the same input pressure of ∼5900 Torr for RF-voltages of 0 V, 20 V, and 77 V (peak-to-peak). The result of the individual scans is shown in Figures 4.7 to 4.9 with count rate and downstream pressure in chambers C and D combined in one plot. The pressure minimum in chambers C and D is reached at a stagnation pressure in chamber B of 0.6-0.7 Torr. In this pressure range the count rate peaks in coincidence with the downstream minimum if a RF amplitude is applied to the funnel (Figures 4.8 and 4.9). The applied RF-amplitude has the largest impact on the transmission here. At higher stagnation pressures the count rate peaks again, however, the location of this count-rate maximum also depends on the applied RF amplitude. If no RF is applied, the maximum peaks at 2 Torr. When 20 V_{PP} are applied the maximum is shifted to 2.7 Torr and to 3.9 Torr for an RF amplitude of 77 V_{PP}. A comparison of the three RF-amplitudes at ∼5900 Torr is shown in Fig. 4.10. The increase of count rate at increased RF amplitudes is clearly visible. The ratio of the amplitude of the peak at 0.6-0.7 Torr to the base count rate increases for increasing RF-amplitudes. This is expected due to the deeper confining potential of the increased RF amplitude.

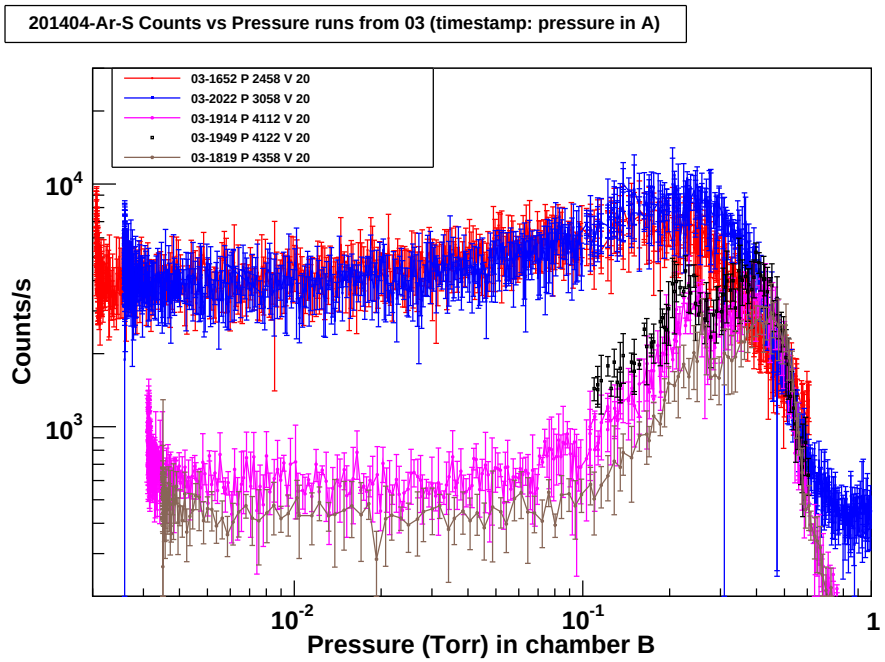

(a) April 3rd 2014.

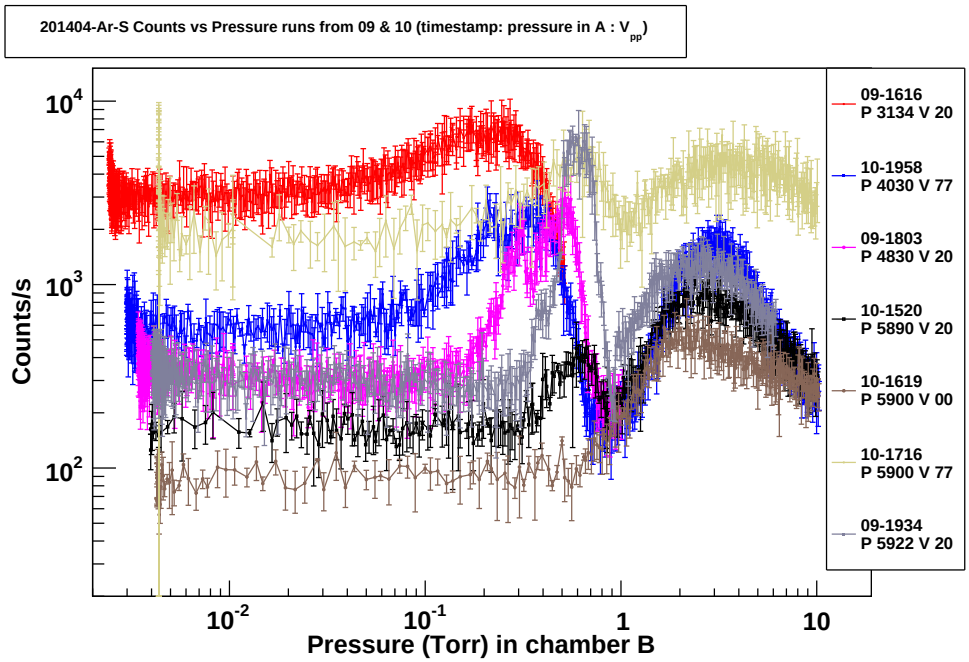

(b) April 9th/10th 2014.

Figure 4.6: Count rate as function of pressure in chamber B for various input pressures. The label is again **dd-hhmm P** *pressure* **V** V_{PP} *on funnel* at 2.6 MHz.

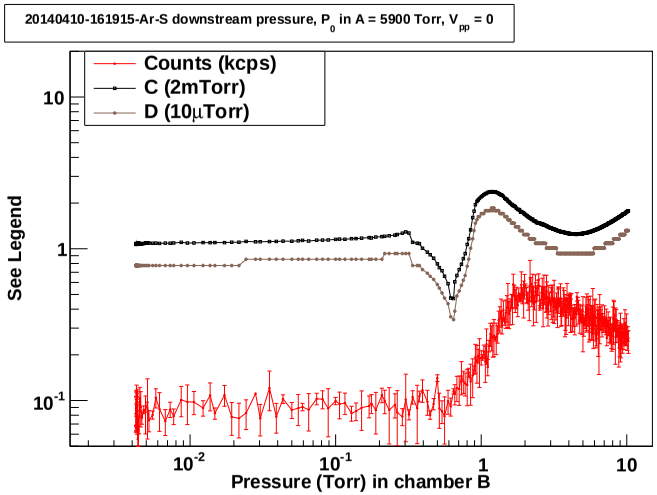

Figure 4.7: RF-funnel amplitude: 0 V.

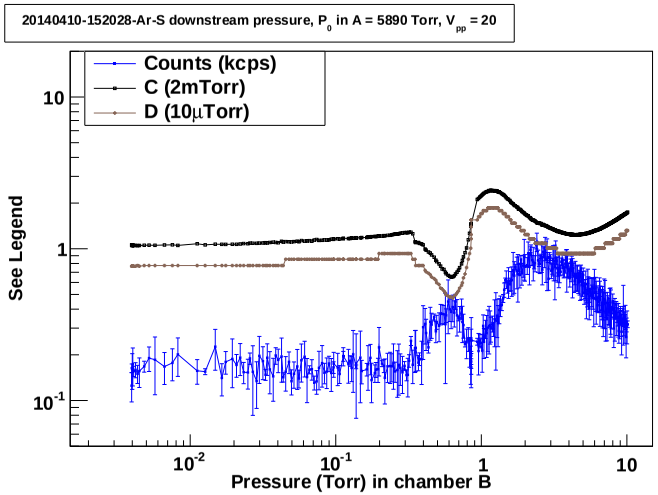

Figure 4.8: RF-funnel amplitude: 20 V.

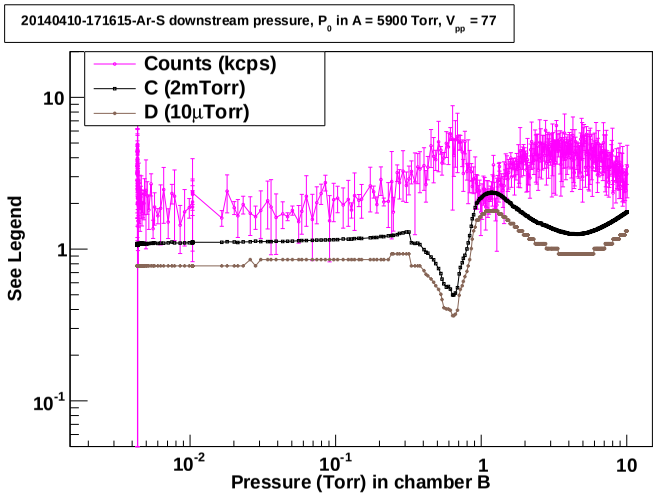

Figure 4.9: RF-funnel amplitude: 77 V.

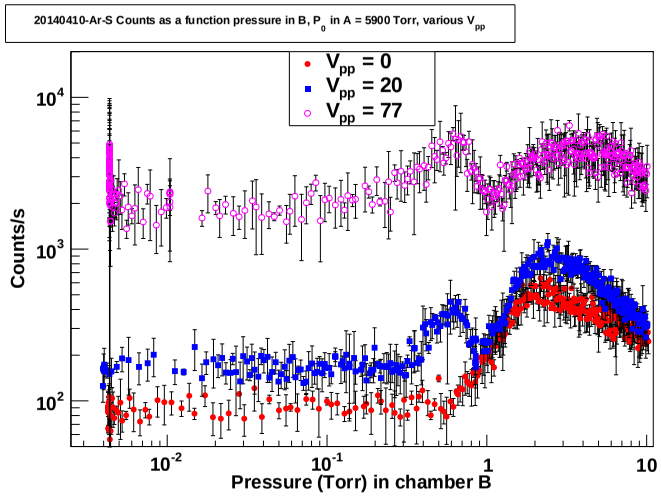

Figure 4.10: Count rate versus pressure in chamber B.

Count rate and pressure in chambers C and D as function of pressure in chamber B. The RF amplitude applied to the funnel is listed under each plot. The input pressure was ∼5900 Torr.

4.4 RF-amplitude scan in Argon

Similar to the measurements presented in Section 3, the RF-amplitude has been varied during some of the scans. It is pointed out that all settings were kept constant during these measurements except the RF-amplitude of the voltages applied to the RF funnel. Prior to a scan the cryo pump cooled down and the measurement was operated in a pressure regime in chamber B where the count rate and the downstream pressures in chambers C and D were constant. Before the RF-amplitude was scanned, the count rate was allowed to stabilize, i.e., the gas flow patterns inside the funnel stabilized (the count rate peaks shortly after the valve HV4 is opened). Each scan took ∼5 minutes (for the complete scan of all amplitudes at a given pressure). The result is shown in Fig. 4.11. The RF amplitude was scanned from 0 V_{PP} to ∼98V_{PP} at the pressures of 1545 Torr, 4030 Torr and 5912 Torr in chamber A, respectively.

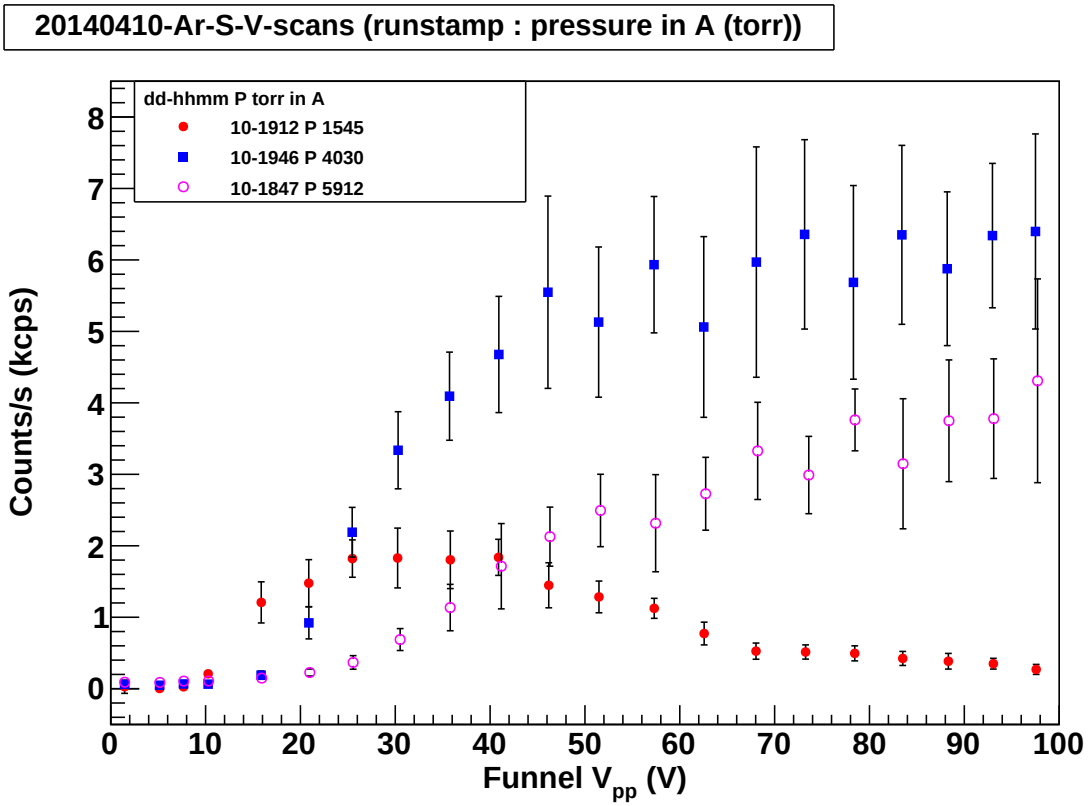

Figure 4.11: CEM count-rate as a function of the applied RF amplitude at 2.6 MHz. The amplitude was scanned at 1545 Torr, 4030 Torr, and 5912 Torr, respectively. Each data point was integrated for 12 seconds

5 Conclusion

Over the last several months some aspects of the funnel operation have been probed. Initial tests investigated the number of ions coming from the funnel as a function of the funnel's RF amplitude and frequency (focused on 2.6 MHz), input pressure in chamber A, and the ambient stagnation

pressure in chamber B. Tests were also performed in order to understand the behavior of the SPIG and the downstream ion optics in chamber D were optimized.

A gas jet was successfully operated with Xenon gas and Argon gas in different modes of operation, i.e., in recovery and non-recovery mode. Most recent measurements with Ar at varying stagnation pressures showed an interesting behavior of pressure in the downstream chambers C and D as well as of the ion-count rate on the CEM. It appears that the maximum transmission of ions can be achieved at $\sim$0.7 Torr in chamber B (for 5900 Torr input pressure). At this pressure, the ion-count rate is the most sensitive to an increasing confining RF field at the funnel and thus the transmission improves the most in this pressure region. Also at this pressure, the downstream pressure is at a minimum.

In preparation of m/q detection with a RGA an electrostatic lens configuration has been added in chamber D. A picture of the most recent lens configuration is shown in Fig. C.10. Here, the CEM is installed past the drift tube. The CEM (not visible in the picture) is installed past the drift tube on the other side of an isolation flange. Prior to all tests with RGAs, the ion optics were optimized with a CEM installed at the later location of the RGA.

Unfortunately, all attempts to inject ions into a RGA for m/q identification were without success so far. In the last quarter of 2013 MKS provided a MicroVision2 (MV2) RGA unit for loan. The ion source of this unit was removed and attempts were made to inject ions into the quadrupole structure. Mass scans were performed at masses 0.5 amu and various masses one would expect in the gas jet such as Argon, Barium, Carbon, Xenon, Gadolinium, and others. One plausible explanation why ions could not be injected into the RGA was an energy miss-match between ion energy (which is negative with respect to ground potential) and RGA. In order to overcome this miss-match a MKS e-Vision$^+$ RGA has been modified and installed in the system downstream of a ceramic HV breaker. In this configuration, the RGA ground potential can be changed with respect to the chamber ground potential. A biased drift tube bridges the gap in the ion flight path that is created by the ceramic breaker. In further tests the RGA was biased at various negative voltages while mass scans were recorded. No positive signal could be found for various ion optic's tuning parameters. A picture of the recently installed MKS EV$^+$ prior to its installation in the system is shown in Fig. C.11.

After the presented measurements with the RF funnel, the focus now lies on the development of means to determine m/q. This is vital to determine the nature of the detected ions and investigate the influence of various operational parameters on different ion masses. This will then lead to the extraction of Ba-ions from high pressure Xe (and Ar) gas (of up to 12 bar).

A Run list

Date	Start Time HHMMSS	Pressure [Torr]	Parameter scanned
2014-04-03	165246	2458	SP ch. B
2014-04-03	181917	4358	SP ch. B
2014-04-03	191404	4112	SP ch. B
2014-04-03	194950	4122	SP ch. B
2014-04-03	202258	3058	SP ch. B
Setup vented with Ar, chicanes installed, signal amplification changed			
2014-04-09	161656	3134	SP ch. B
2014-04-09	180357	4830	SP ch. B
2014-04-09	193432	5922	SP ch. B†
Cryo pump temperature cycled			
2014-04-10	152028	5890	SP ch. B with V_{PP}=20 V
2014-04-10	161915	5905	SP ch. B with V_{PP}=0 V
2014-04-10	171615	5900	SP ch. B with V_{PP}=77 V
2014-04-10	184739	5912	RF-amplitude on funnel
2014-04-10	191228	1545	RF-amplitude on funnel
2014-04-10	191942	1555	too little gas flow to scan SP
2014-04-10	194640	4030	RF-amplitude on funnel
2014-04-10	195836	4030	SP ch. B with V_{PP}=77 V

Table A.1: List of runs with date, time and pressure in chamber A. Typically, the stagnation pressure (SP) in chamber B was scanned. If not noted or scanned, V_{PP}=20 V was applied.
† This run has the largest spike in count rate at ∼1 Torr stagnation pressure. The result could not be reproduced.

B Graphs

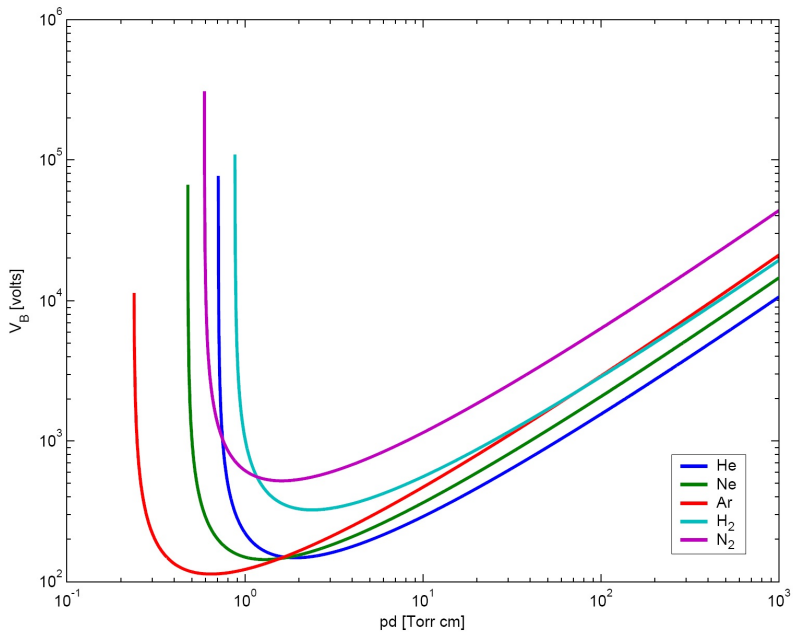

Figure B.1: Paschen curve for various gasses. In all measurements that are presented in this document the voltages on the funnel stayed well below 100 V_{PP}. Graph taken from Wikipedia.

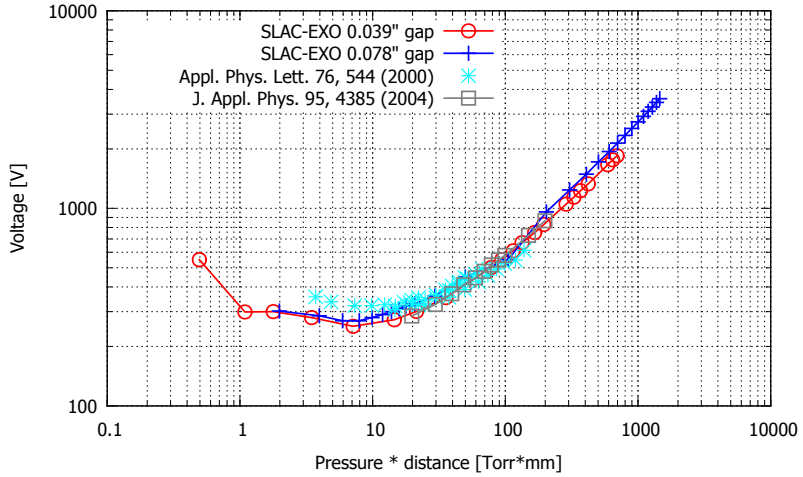

Figure B.2: Paschen curve for Xenon. The source of the data point is listed in the legend. The red and blue data points were recorded at SLAC using a 1 mm (0.039") and 2 mm (0.078") gap, respectively.

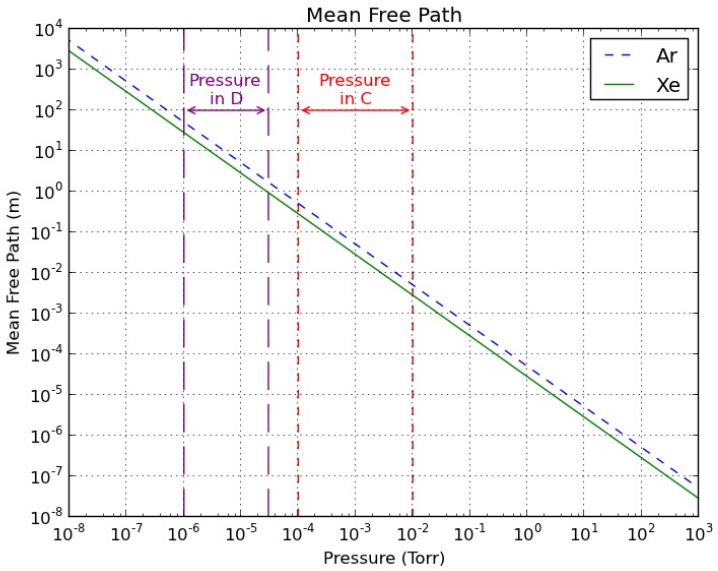

Figure B.3: Mean free path in Argon and Xenon at various pressures. The pressure ranges during gas jet operation in chambers C and D are indicated in red and violet, respectively.

C Pictures

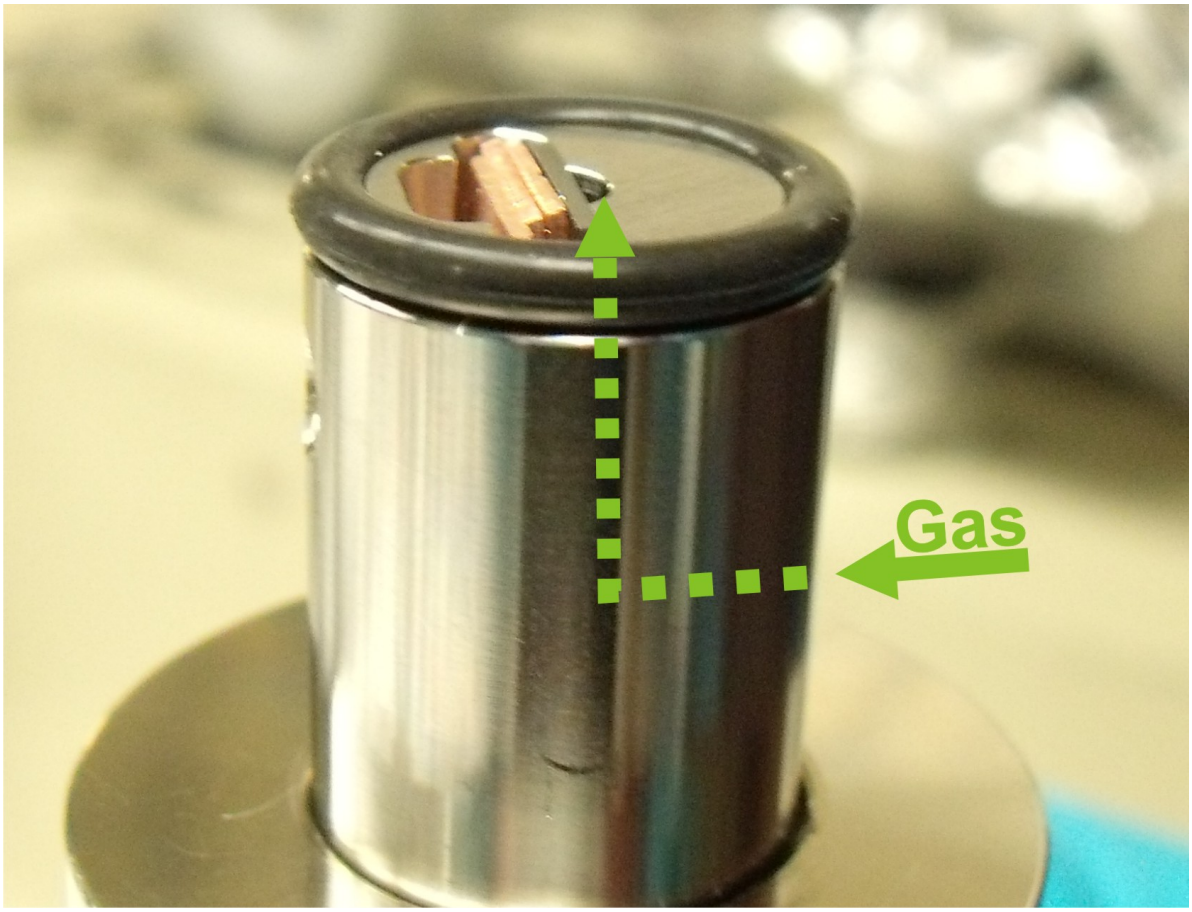

Figure C.1: Picture of the source holder with (stainless steel) source plate. The copper plated are backing the source plate. The gas enters the source holder from the side and flows along the surface of the source plate. The gas path is indicated by the dashed arrow. When mounted, the source holder presses into the back of the converging-diverging nozzle, sealing along the viton gasket, so that the entrance of the nozzle is where the tip of the dashed arrow ends.

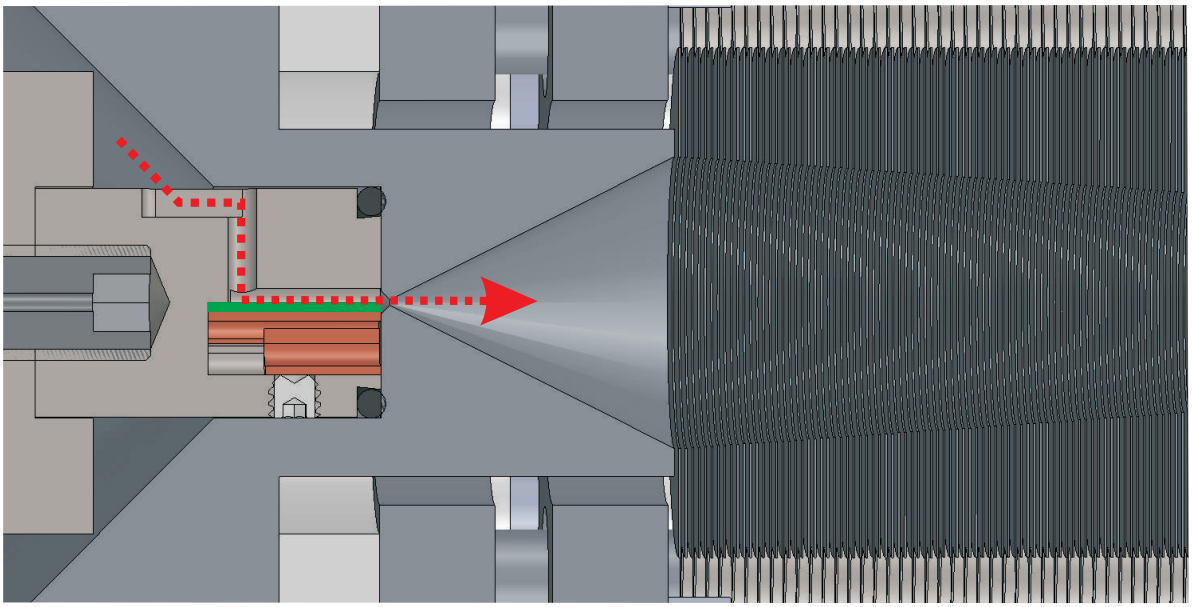

Figure C.2: Section view of the source holder installed in the setup. The source plate is highlighted in green. A red dashed arrow indicates the gas flow direction. The gas flows across the source surface before it enters the converging-diverging nozzle. The start of the RF funnel is visible on the right side.

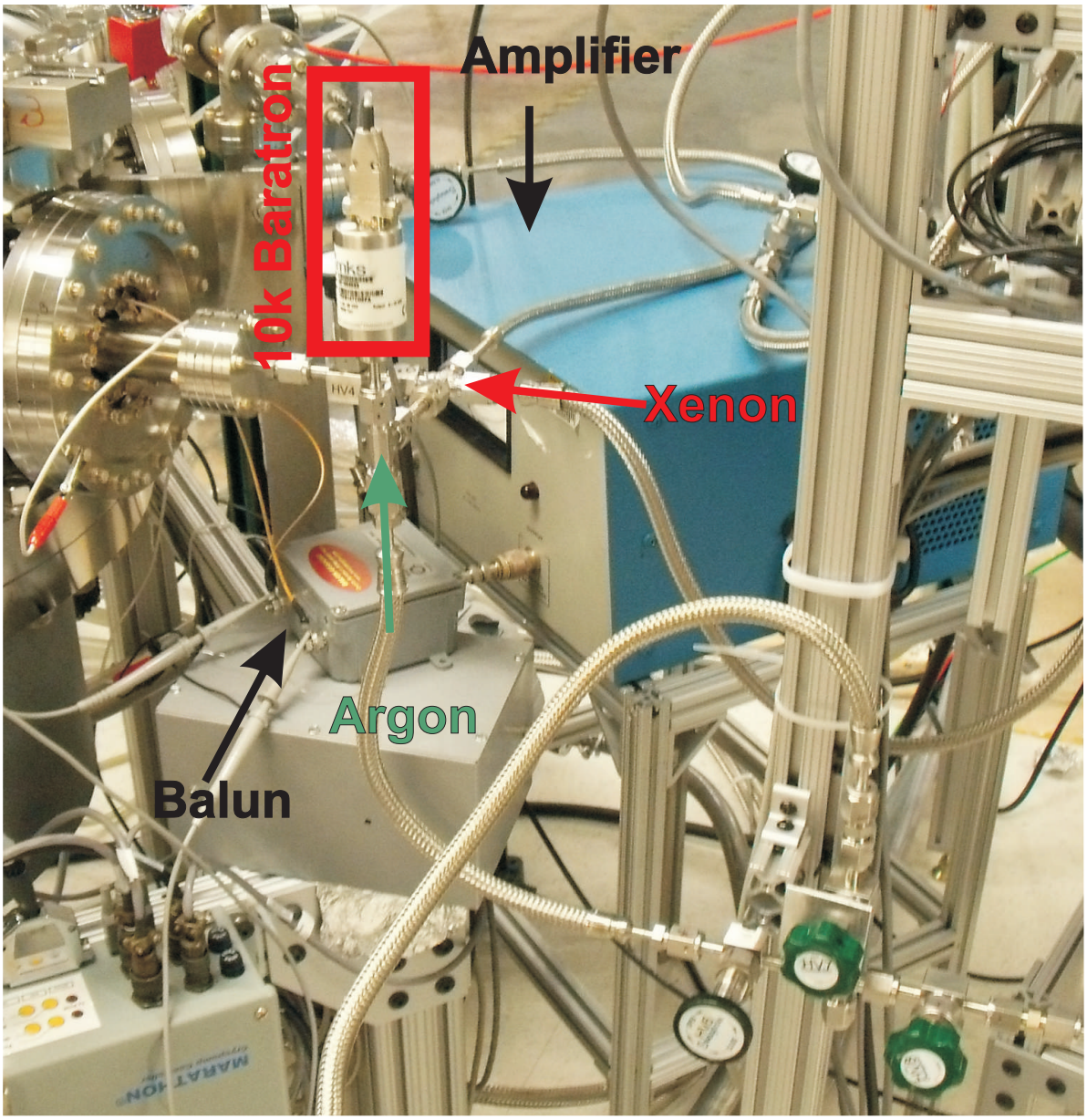

Figure C.3: Picture of the amplifier and the balun setup. Also indicated is the 10 kTorr Baratron that reads the pressure in chamber A.

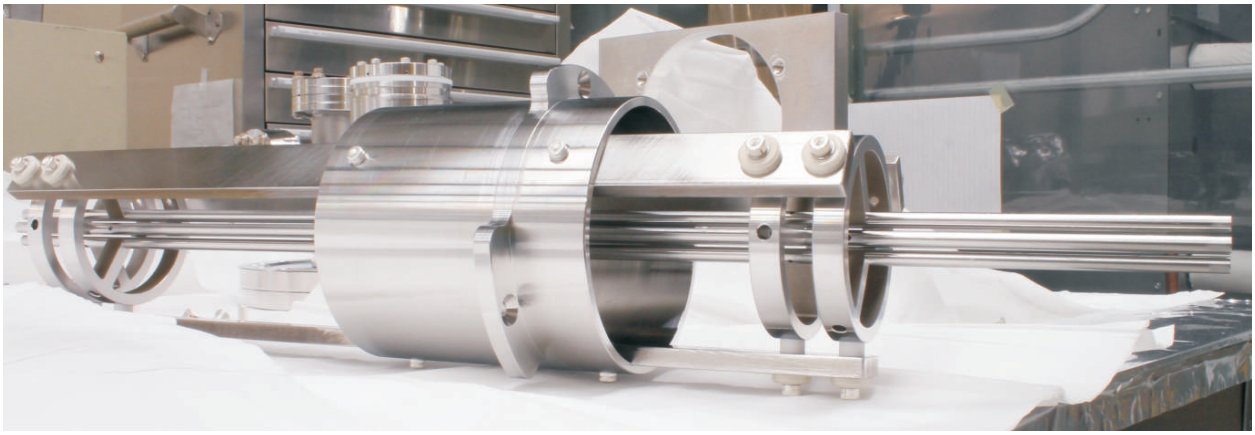

Figure C.4: Picture of the sextupole ion guide (SPIG) prior to installation. Each set of three rods forming an electrode is mounted to the circular positioning holder at both ends. These holders are supported between the bars mounted to the central mount. The rods are 480.5 mm long.

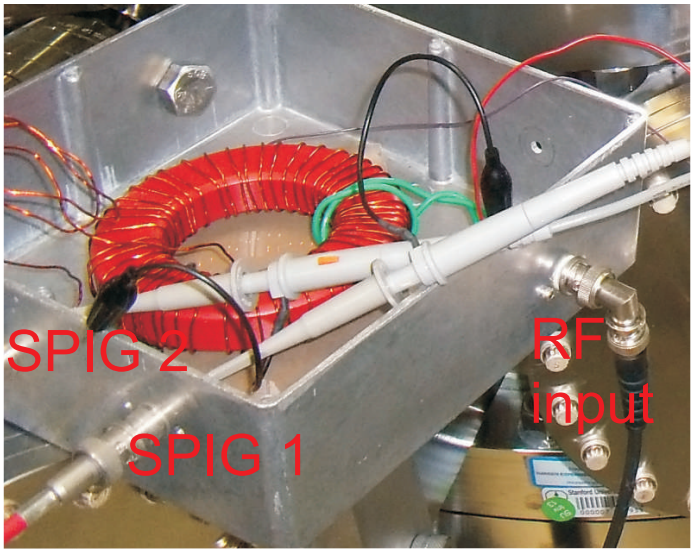

Figure C.5: Picture of the toroidal transformer that supplies the SPIG. The RF is supplied through the BNC cable and each phase of the SPIG is connected to the connector labeled SPIG 1 and 2.

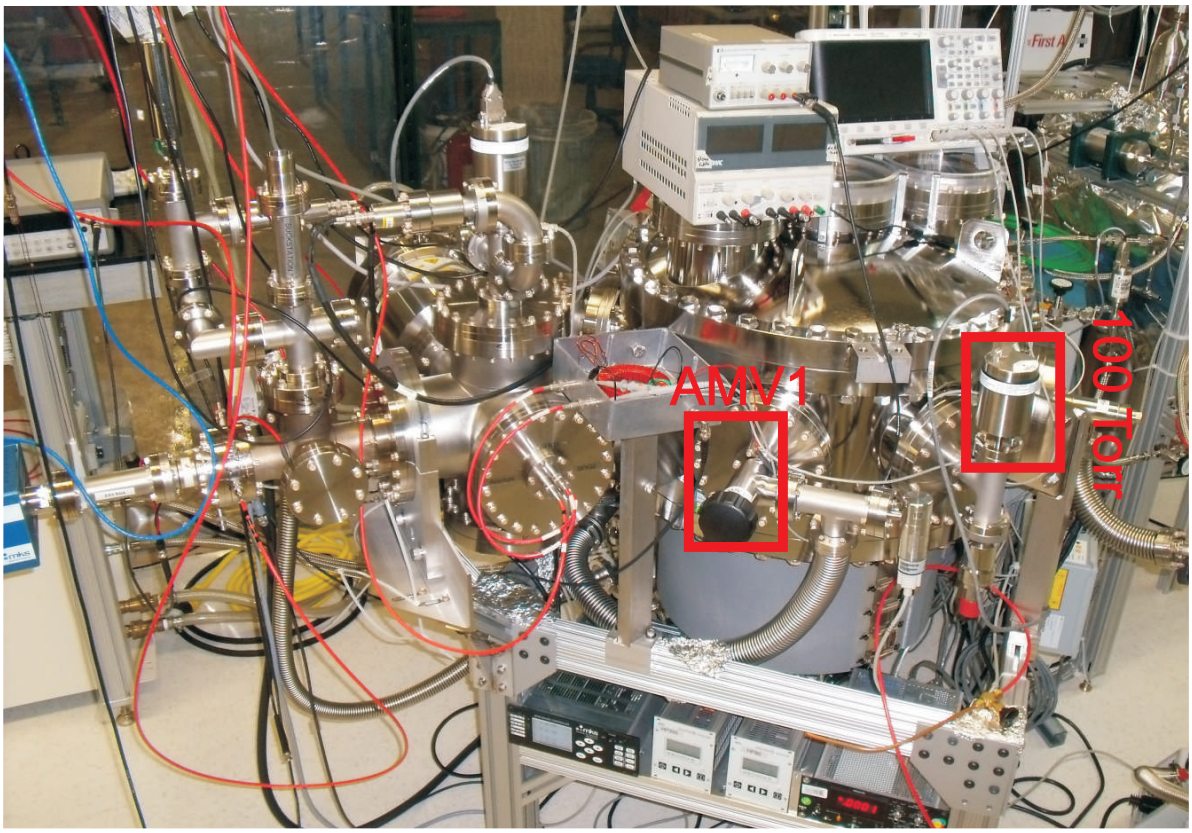

Figure C.6: Picture of chamber B. The location of the 100 Torr Baratron is indicated by a red rectangle. The funnel is installed in the center of Chamber B parallel to the three ports on top of the chamber (used as stand for scope and power supplies). Also highlighted is all-metal-valve 1 (AMV1) that connects the backing lines of ML and HP80 to chamber B. In non-recovery mode this valve is closed.

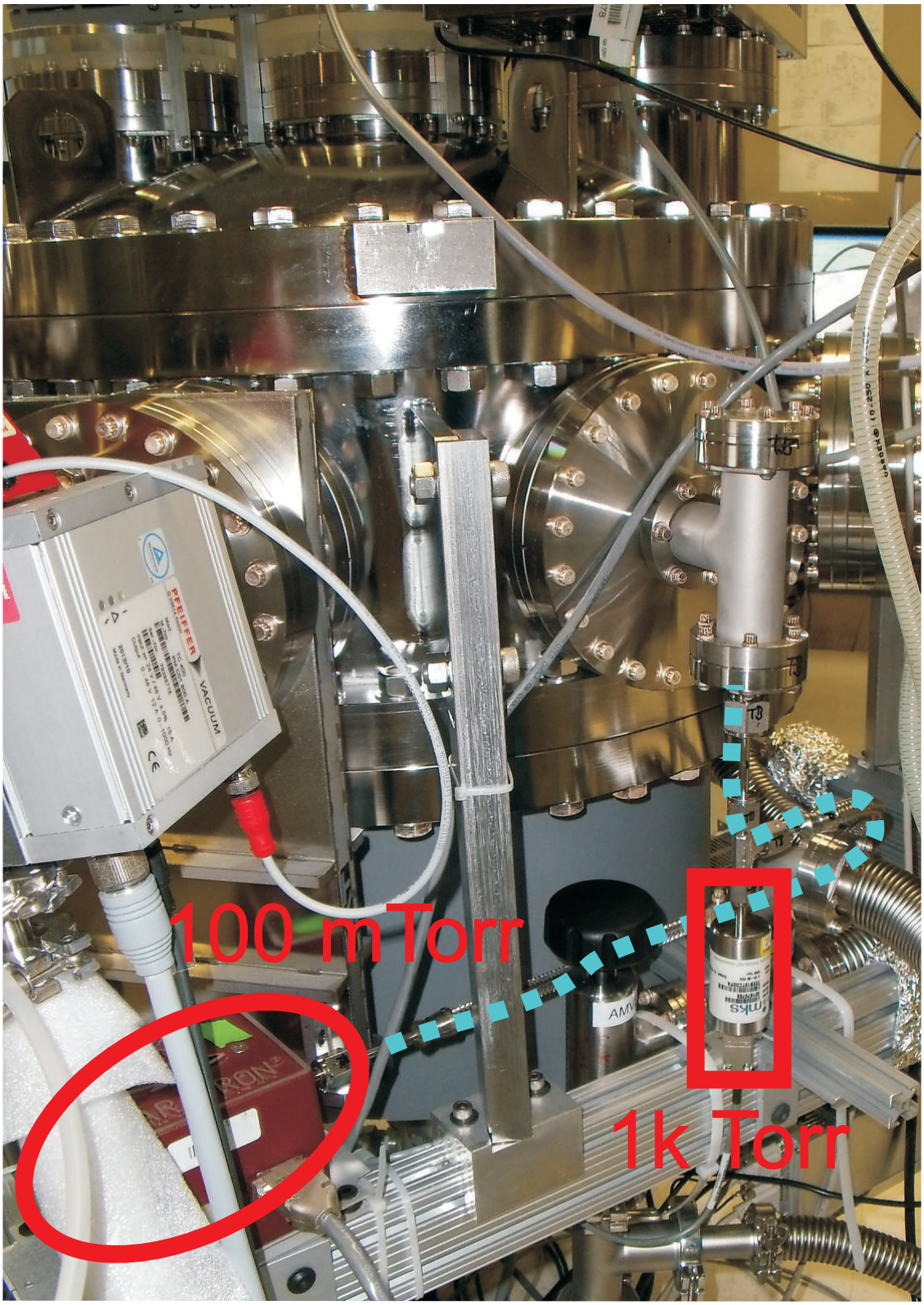

Figure C.7: Picture of chamber B. The location of 100 mTorr and 1 kTorr Baratron is indicated in red. The blue dashed line highlights the 1/2" VCR line that connects the 0.1 Torr Baratron to chamber B.

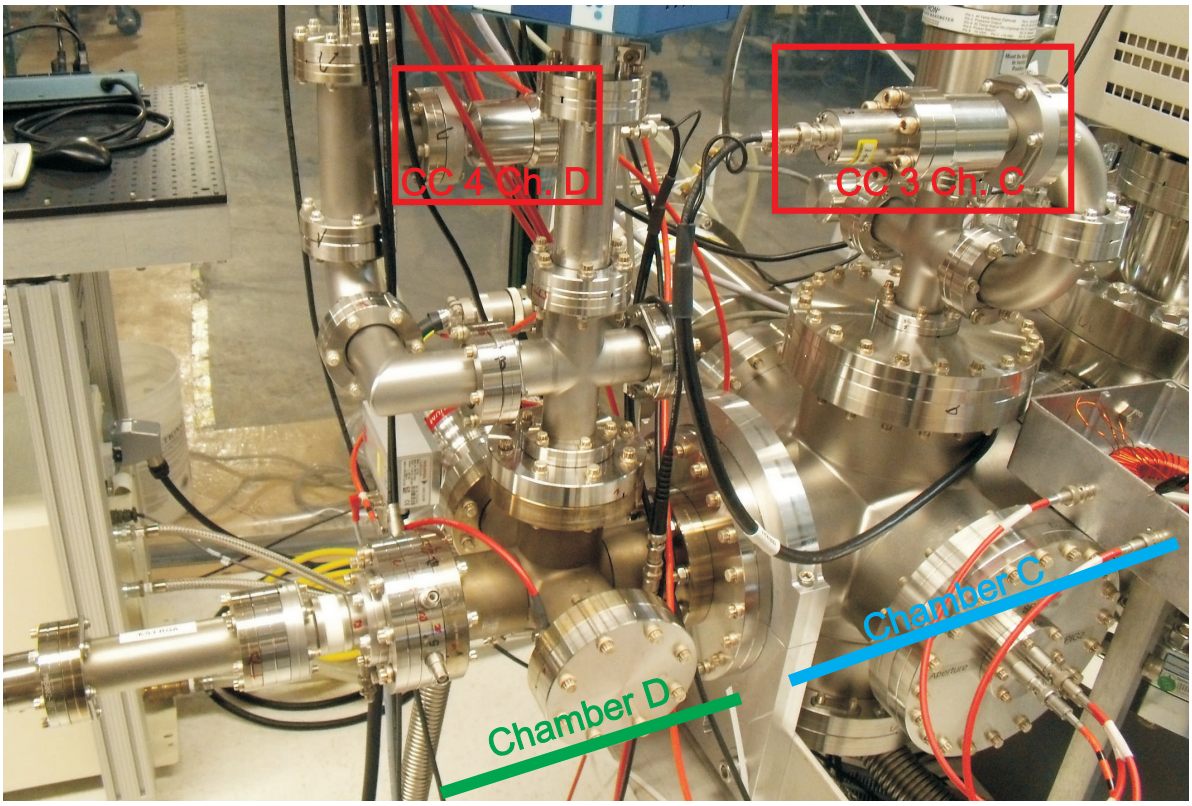

Figure C.8: Picture of the cold cathode gauges on chambers C and D. They are both mounted after at least two 90° bends. These additional chicanes prevent cold cathode induced counts on the CEM.

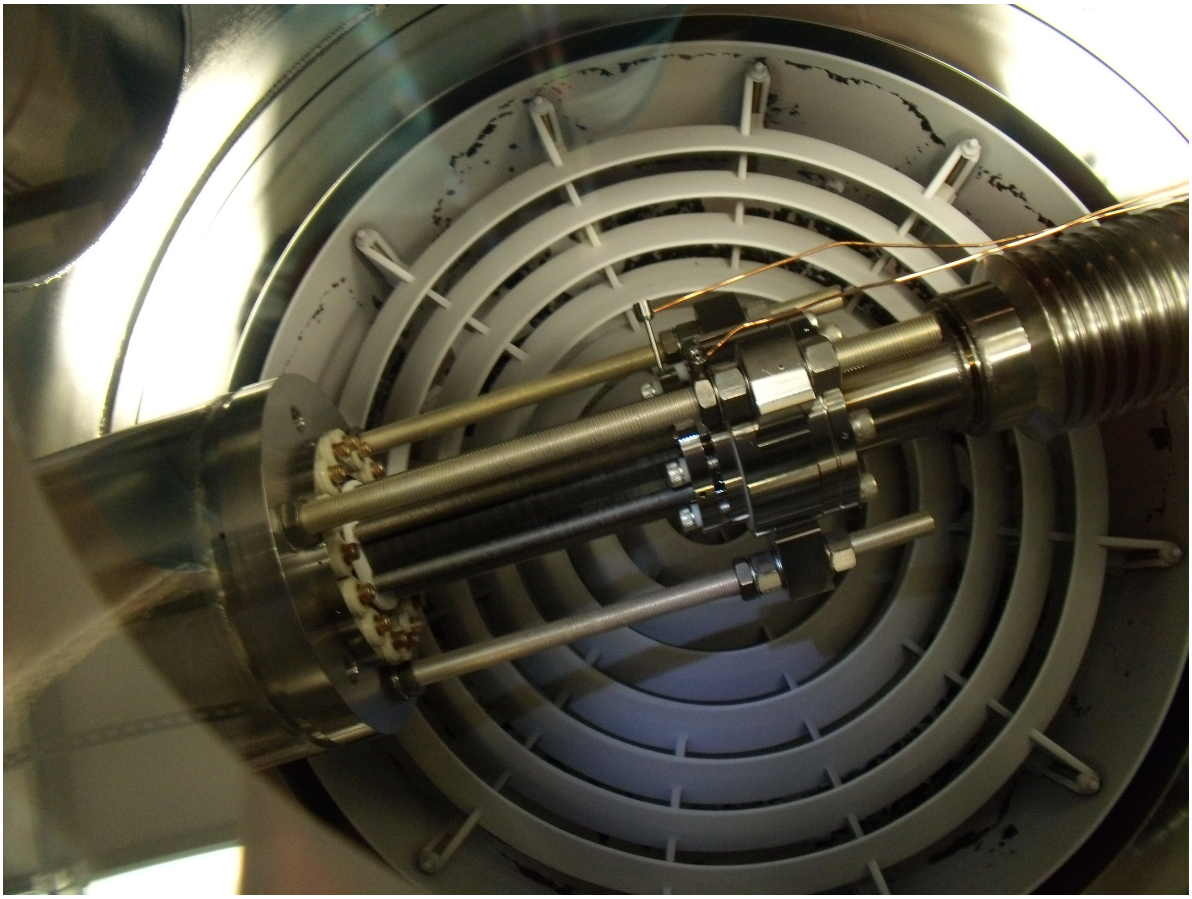

Figure C.9: Picture of the funnel installed in chamber B. The picture is taken during Xe gas operations through a window installed at the top center flange in the lid of chamber B. The white on the cryo pump's first stage and the wall is Xe ice (the natural color of the cryo pump's stages is stainless steel and the walls are typically black).

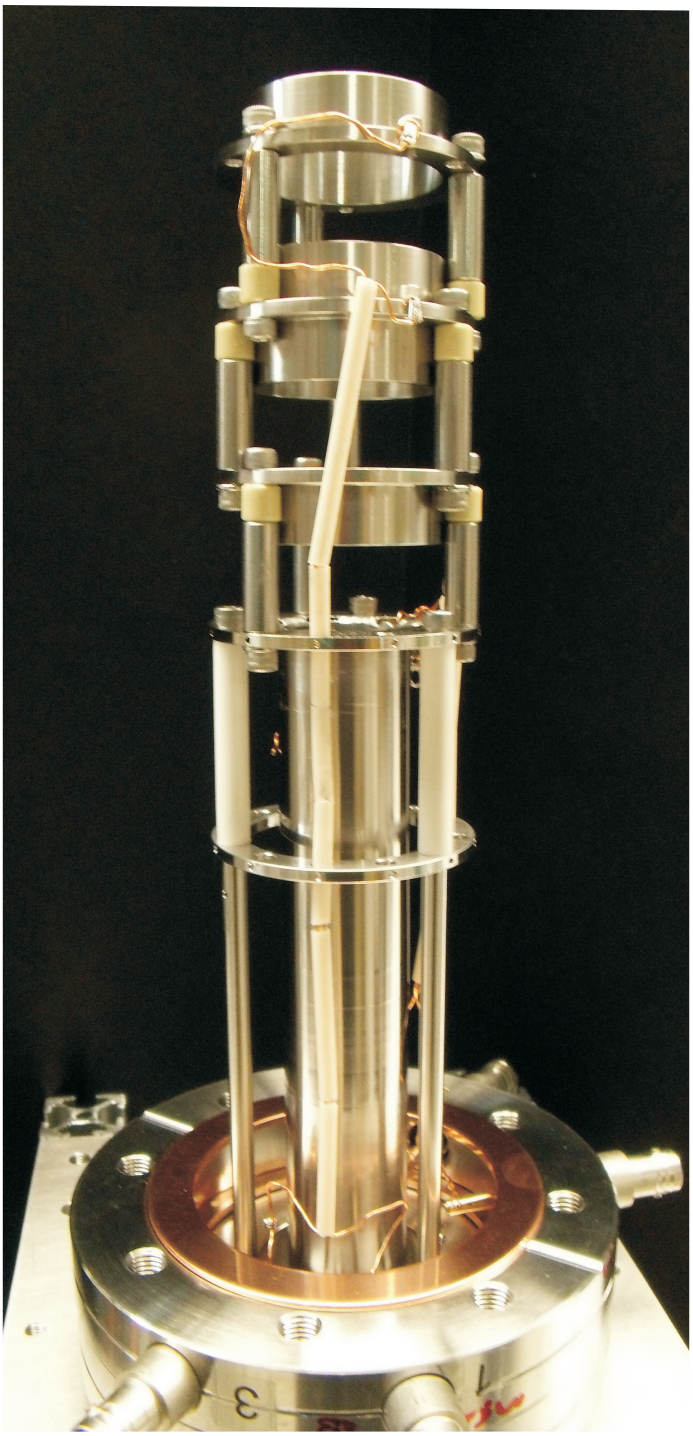

Figure C.10: Picture of the lens assembly that is currently installed in chamber D. The current setup consists of three lenses and one drift tube. In this most recent assembly stainless steel standoffs were used to reduce the exposure of ceramic parts to the beam. CEM or RGA are installed after an isolation flange, see Fig. C.8.

Figure C.11: Picture of the RGS head without ion source. The leads that connected to the ion source were bent backwards and are electrically isolated by a Kapton foil. The lens with the mesh at the center of the picture is biased at -115 V with respect to ground.